VERIFICATION OF FUNCTIONAL A POSTERIORI ERROR ESTIMATES FOR OBSTACLE PROBLEM IN 2D

Petr Harasim and Jan Valdman

We verify functional a posteriori error estimates proposed by S. Repin for a class of obstacle problems in two space dimensions. New benchmarks with known analytical solution are constructed based on one dimensional benchmark introduced by P. Harasim and J. Valdman. Numerical approximation of the solution of the obstacle problem is obtained by the finite element method using bilinear elements on a rectangular mesh. Error of the approximation is measured by a functional majorant. The majorant value contains three unknown fields: a gradient field discretized by Raviart–Thomas elements, Lagrange multipliers field discretized by piecewise constant functions and a scalar parameter β. The minimization of the majorant value is realized by an alternate minimization algorithm, whose convergence is discussed. Numerical results validate two estimates, the energy estimate bounding the error of approximation in the energy norm by the difference of energies of discrete and exact solutions and the majorant estimate bounding the difference of energies of discrete and exact solutions by the value of the functional majorant.

Keywords: obstacle problem, a posteriori error estimate, functional majorant, finite element method, variational inequalities, Raviart–Thomas elements

Classification: 34B15, 65K15, 65L60, 74K05, 74M15, 74S05

1. INTRODUCTION

Problems with obstacles often arise in continuum mechanics. Their mathematical models are often formulated in terms of variational inequalities [11, 14]. Typically, numerical treatment of obstacle problems is obtained by the finite element method combined with methods developed for convex minimization problems with constraints. It was traditionally tackled by the Uzawa method, the interior point method, the active set method with gradient splitting and the semi-smooth Newton method among others, see, e.g., [8, 26].

A priori analysis providing asymptotic estimates of the quality of finite elements approximations converging toward the exact solution was studied for obstacle problems e.g. in [5, 9]. For the survey of the most important techniques in a posteriori analysis (such as residual, gradient averaging or equilibration methods) we refer to the monographs [1, 2, 3]. Particular a posteriori estimates for variational inequalities including

a obstacle problem are reported e. g. in [4, 7, 28] among others.

Our goal is to verify guaranteed functional a posteriori estimates expressed in terms of functional majorants derived by Repin [17, 23]. The functional majorant upper bounds are essentially different with respect to known a posteriori error estimates mentioned above. The estimates are obtained with the help of variational (duality) method which was developed in [20, 21] for convex variational problems. The method was applied to various nonlinear models including those associated with variational inequalities [22], in particular problems with obstacles [6], problems generated by plasticity theory [10, 25] and problems with nonlinear boundary conditions [24].

Three benchmarks with known analytical solution of the obstacle problem are considered in numerical experiments. For a known benchmark introduced in [18] constructed on a square domain assuming non-zero Dirichlet boundary conditions and a constant obstacle, values of exact energy and Lagrange multipliers are added. Two new benchmarks are constructed on a ring domain assuming zero Dirichlet boundary conditions and either constant or spherical obstacle. The construction was inspired by a one dimensional benchmark from [13].

Numerical tests has been performed using Matlab code providing a bilinear approximation of the obstacle problems on uniform rectangles, Raviart–Thomas approximation of the gradient field and piecewise constant approximation of the Lagrange multiplier field. The code is vectorized in manner of [19] to provide a fast computation of finer mesh rectangulations.

Outline of the paper is as follows. In Section 2, we formulate a constrained minimization problem, a perturbed minimization problem and explain how to derive a functional a posteriori error estimate. Benchmarks with known analytical solution are discussed in Section 3. Numerical tests performed in Matlab are reported in Section 4. Additional details of the finite element implementation are mentioned in Appendix.

2. OBSTACLE PROBLEM AND A POSTERIORI ERROR ESTIMATE

Throughout the paper, $\Omega \subset \mathbb{R}^2$ denotes a bounded domain with Lipschitz continuous boundary $\partial\Omega$,

$$V = H^1(\Omega)$$

stands for the standard Sobolev space and

$$V_0 = H_0^1(\Omega)$$

denotes its subspace consisting of functions vanishing on the boundary $\partial\Omega$. We deal with the abstract obstacle problem, described by the following minimization problem:

Problem 1. Find $u \in K$ satisfying

$$J(u) = \inf_{v \in K} J(v), \tag{1}$$

where the energy functional reads

$$J(v) := \frac{1}{2} \int_\Omega \nabla v \cdot \nabla v \, \mathrm{d}x - \int_\Omega f v \, \mathrm{d}x \tag{2}$$

and the set of admissible functions is defined as

$$K := \{v \in V_0 : v(x) \geq \phi(x) \text{ a.e. in } \Omega\}.$$

Here, $f \in L^2(\Omega)$ denotes a loading function and $\phi \in V$ an obstacle function satisfying $\phi(x) < 0$ on $\partial\Omega$.

Problem 1 is a quadratic minimization problem with a convex constraint and the existence of its minimizer is guaranteed by convexity, coercivity and lower semicontinuity of the functional J [16]. It is equivalent to the following variational inequality: Find $u \in K$ such that

$$\int_\Omega \nabla u \cdot \nabla(v - u)\mathrm{d}x \geq \int_\Omega f(v - u)\mathrm{d}x \quad \text{for all } v \in K. \tag{3}$$

The convex constraint $v \in K$ can be transformed into a linear term containing a new (Lagrange) variable in

Problem 2. (Perturbed problem) For given

$$\mu \in \Lambda := \{\mu \in L^2(\Omega) : \mu \geq 0 \text{ a.e. in } \Omega\}$$

find $u_\mu \in V_0$ such that

$$J_\mu(u_\mu) = \inf_{v \in V_0} J_\mu(v), \tag{4}$$

where the perturbed functional J_μ is defined as

$$J_\mu(v) := J(v) - \int_\Omega \mu(v - \phi)\,\mathrm{d}x. \tag{5}$$

Problems 1 and 2 are related and it obviously holds

$$J_\mu(u_\mu) \leq J(u) \quad \text{for all } \mu \in \Lambda. \tag{6}$$

Remark 2.1. (Existence of optimal multiplier) If u has a higher regularity,

$$u \in V_0 \cap H^2(\Omega), \tag{7}$$

there exists an optimal multiplier $\lambda \in \Lambda$ such that $u_\lambda = u$ and $J_\lambda(u) = J(u)$. Moreover, it holds

$$\lambda = -(\Delta u + f). \tag{8}$$

For more details, see [13, Lemma 2.1 and Remark 2.3].

Remark 2.2. (Higher regularity of solution) If f and ϕ have higher regularity, e. g., if $f \in C(\overline{\Omega})$ and $\phi \in C^1(\overline{\Omega})$, then (7) holds and even $u \in C^1(\overline{\Omega})$. For more details, see e. g. [12, 15].

We are interested in analysis and numerical properties of the a posteriori error estimate of numerical solution $v \in K$ to Problem 1 in the energy norm

$$\|v\|_E := \left(\int_\Omega \nabla v \cdot \nabla v \, \mathrm{d}x \right)^{\frac{1}{2}}.$$

The following part is based on results of S. Repin et al. [6, 17, 22]. It is easy to see that

$$J(v) - J(u) = \frac{1}{2}\|v - u\|_E^2 + \int_\Omega \nabla u \cdot \nabla(v - u) \, \mathrm{d}x - \int_\Omega f(v - u)\mathrm{d}x \qquad \text{for all } v \in K \quad (9)$$

and (3) implies an energy estimate

$$\frac{1}{2}\|v - u\|_E^2 \le J(v) - J(u) \quad \text{for all } v \in K. \tag{10}$$

Quality of (10) is tested in Section 4 for several problems with known exact solution $u \in K$ introduced in Section 3. By using (6), we obtain the estimate

$$J(v) - J(u) \le J(v) - J_\mu(u_\mu) \quad \text{for all } \mu \in \Lambda. \tag{11}$$

In [17], the right hand side of (11) is further estimated by a majorant estimate

$$J(v) - J(u) \le \mathcal{M}(v, f, \phi; \beta, \mu, \tau^*) \tag{12}$$

valid for all $\beta > 0, \mu \in \Lambda, \tau^* \in H(\Omega, \mathrm{div})$. The flux variable τ^* is defined in the space

$$H(\Omega, \mathrm{div}) := \{\tau^* \in [L^2(\Omega)]^2 : \mathrm{div}\, \tau^* \in L^2(\Omega)\}$$

well studied in various mixed problems. The right-hand side of (12) denotes a functional majorant

$$\mathcal{M}(v, f, \phi; \beta, \mu, \tau^*) := \frac{1+\beta}{2}\|\nabla v - \tau^*\|_\Omega^2 + \frac{1}{2}\left(1 + \frac{1}{\beta}\right)C_\Omega^2\|\mathrm{div}\,\tau^* + f + \mu\|_\Omega^2$$

$$+ \int_\Omega \mu(v - \phi)\mathrm{d}x. \quad (13)$$

Here, the corresponding Ω-norms of scalar and vector arguments read

$$\|v\|_\Omega := \left(\int_\Omega v^2 \, \mathrm{d}x \right)^{1/2} \qquad \text{for all } v \in L^2(\Omega),$$

$$\|\tau^*\|_\Omega := \left(\int_\Omega \tau^* \cdot \tau^* \, \mathrm{d}x \right)^{1/2} \qquad \text{for all } \tau^* \in L^2(\Omega, \mathbb{R}^d)$$

and a constant $C_\Omega > 0$ represents an upper bound of constant in the Friedrichs inequality

$$\|v\|_\Omega \le C_\Omega\|\nabla v\|_\Omega$$

valid for all $v \in V_0$. For more details on derivation of the majorant estimate (12), we refer to [17].

Remark 2.3. If the assumption (7) is fulfilled, there exist optimal majorant parameters $\tau_{\mathrm{opt}}^* = \nabla u$, $\mu_{\mathrm{opt}} = \lambda \in \Lambda$ and $\beta_{\mathrm{opt}} \to 0$ such that the inequality in (12) changes to equality, i. e. the majorant on right-hand side of (12) defines the difference of energies $J(v) - J(u)$ exactly (see [13, Lemma 3.4]).

Our goal is to find unknown optimal parameters β_{opt}, μ_{opt} and τ_{opt}^* which minimizes the majorant.

Problem 3. (Majorant minimization problem) Let $v \in K$, $f \in L^2(\Omega)$, $\phi < 0$ be given. Find

$$(\beta_{\mathrm{opt}}, \mu_{\mathrm{opt}}, \tau_{\mathrm{opt}}^*) = \operatorname*{argmin}_{\beta, \mu, \tau^*} \mathcal{M}(v, f, \phi; \beta, \mu, \tau^*)$$

over arguments $\beta > 0, \mu \in \Lambda, \tau^* \in H(\Omega, \mathrm{div})$.

Algorithm 1 Majorant minimization algorithm.

Let $k = 0$ and let $\beta_0 > 0$ and $\mu_0 \in \Lambda$ be given. Then:

  (i) find $\tau_{k+1}^* \in H(\Omega, \mathrm{div})$ such that

$$\tau_{k+1}^* = \operatorname*{argmin}_{\tau^* \in H(\Omega, \mathrm{div})} \mathcal{M}(v, f, \phi; \beta_k, \mu_k, \tau^*),$$

  (ii) find $\mu_{k+1} \in \Lambda$ such that

$$\mu_{k+1} = \operatorname*{argmin}_{\mu \in \Lambda} \mathcal{M}(v, f, \phi; \beta_k, \mu, \tau_{k+1}^*),$$

  (iii) find $\beta_{k+1} > 0$ such that

$$\beta_{k+1} = \operatorname*{argmin}_{\beta > 0} \mathcal{M}(v, f, \phi; \beta, \mu_{k+1}, \tau_{k+1}^*),$$

  (iv) set $k := k + 1$ are repeat (i)–(iii) until convergence.

  (v) output $\tau^* := \tau_{k+1}^*$ and $\mu := \mu_{k+1}$.

We apply Algorithm 1 from [13] to solve Problem 3. The minimization in step (i) is equivalent to the following variational equation: Find $\tau_{k+1}^* \in H(\Omega, \mathrm{div})$ such that

$$(1 + \beta_k) \int_\Omega \tau_{k+1}^* \cdot w \mathrm{d}x + \left(1 + \frac{1}{\beta_k}\right) \int_\Omega \mathrm{div}\, \tau_{k+1}^* \mathrm{div}\, w \mathrm{d}x$$

$$= (1 + \beta_k) \int_\Omega \nabla v \cdot w \mathrm{d}x - \left(1 + \frac{1}{\beta_k}\right) \int_\Omega (f + \mu_k) \mathrm{div}\, w \mathrm{d}x \quad \text{for all } w \in H(\Omega, \mathrm{div}). \quad (14)$$

The minimization in step (ii) is equivalent to the variational inequality: Find $\mu_{k+1} \in \Lambda$ such that

$$\int_\Omega \left[\left(1 + \frac{1}{\beta_k}\right) \left(\mathrm{div}\, \tau_{k+1}^* + \mu_{k+1} + f\right) + v - \phi \right] (w - \mu_{k+1}) \mathrm{d}x \geq 0 \quad \text{for all } w \in \Lambda. \quad (15)$$

The minimization in step (iii) leads to the explicit relation

$$\beta_{k+1} = \frac{\|\operatorname{div} \tau^*_{k+1} + f + \mu_{k+1}\|_\Omega}{\|\nabla v - \tau^*_{k+1}\|_\Omega}. \tag{16}$$

Further details on discretization of Algorithm 1 and its discrete convergence are described in Subsection 4.1.

3. EXACT SOLUTIONS OF SOME OBSTACLE PROBLEMS

Three obstacle problems with known analytical solutions are discussed here.

3.1. Benchmark I: square domain, constant obstacle, nonzero Dirichlet BC

This benchmark is taken from [18]. Let us consider a square domain $\Omega = (-1,1)^2$ and prescribe a contact radius $R \in [0,1)$. For loading

$$f(x,y) = \begin{cases} -16(x^2 + y^2) + 8R^2 & \text{if} \quad \sqrt{x^2 + y^2} > R \\ -8(R^4 + R^2) + 8R^2(x^2 + y^2) & \text{if} \quad \sqrt{x^2 + y^2} \le R, \end{cases}$$

it can be shown that

$$u(x,y) = \begin{cases} \left(\max\{x^2 + y^2 - R^2, 0\}\right)^2 & \text{if} \quad (x,y) \in \Omega \\ \left(x^2 + y^2 - R^2\right)^2 & \text{if} \quad (x,y) \in \partial\Omega \end{cases}$$

is the exact solution of Problem 1 in case of the zero obstacle function $\phi = 0$. The corresponding energy reads

$$J(u) = 192\left(\frac{12}{35} - \frac{28R^2}{45} + \frac{R^4}{3}\right) - 32R^2\left(\frac{28}{45} - \frac{4R^2}{3} + R^4\right) + \frac{2}{3}\pi R^8.$$

It is not difficult to show that

$$\nabla u(x,y) = \begin{cases} 4(x^2 + y^2 - R^2)(x,y) & \text{if} \quad \sqrt{x^2 + y^2} > R \\ (0,0) & \text{if} \quad \sqrt{x^2 + y^2} \le R. \end{cases}$$

With respect to (8), the optimal multiplier reads

$$\lambda(x,y) = \begin{cases} 0 & \text{if} \quad \sqrt{x^2 + y^2} > R \\ 8(R^4 + R^2) - 8R^2(x^2 + y^2) & \text{if} \quad \sqrt{x^2 + y^2} \le R. \end{cases}$$

3.2. Benchmarks defined on ring domain

We consider a ring domain $\Omega := \{(x,y) \in \mathbb{R}^2 : x^2 + y^2 < 1\}$ and a constant negative loading f. In case of an inactive obstacle, Problem 1 can be reduced to the following linear boundary value problem: Find a function u such that

$$-\Delta u = f \quad \text{on} \quad \Omega \tag{17}$$

$$u = 0 \quad \text{on} \quad \partial\Omega. \tag{18}$$

The solution of $(17)-(18)$ reads

$$u(x, y) = \frac{f}{4}(1 - x^2 - y^2) \tag{19}$$

and(19) minimizes the original energy functional (2) of Problem 1 in the whole space V_0 (no obstacle constraint is respected) and the corresponding energy reads

$$J(u) = -\frac{\pi f^2}{16}. \tag{20}$$

In the case of an active and radially symmetric obstacle $\phi = \phi(r)$, where

$$r := \sqrt{x^2 + y^2}$$

denotes a radius in polar coordinates, there will be an unknown contact radius $R \in (0, 1)$ depending on the value of f and the shape $\phi = \phi(r)$ only, see Figure 1. In Subsections 3.2.1 and 3.2.2, we consider cases of constant and spherical obstacles. Outside of the contact domain, where $r \in (R, 1)$, the exact solution $u = u(r)$ is radially symmetric and satisfies the equation (17) transformed to polar coordinates and modified boundary conditions

$$\frac{\partial^2 u}{\partial r^2} + \frac{1}{r}\frac{\partial u}{\partial r} = -f \qquad \text{for } r \in (R, 1) \tag{21}$$

$$u(R) = \phi(R) \tag{22}$$

$$u(1) = 0. \tag{23}$$

The solution of $(21)-(23)$ reads

$$u(r) = \frac{4\phi(R) + fR^2 - f}{4 \ln R} \ln r - \frac{fr^2}{4} + \frac{f}{4}. \tag{24}$$

3.2.1. Benchmark II: ring domain, constant obstacle and zero Dirichlet BC

This benchmark generalizes 1D benchmark from [13] into 2D. We consider a constant negative obstacle function ϕ. It follows from (19), the obstacle is inactive for smaller loadings satisfying

$$|f| < 4|\phi|.$$

Thus, the exact solution of Problem 1 is given by (19) and the corresponding energy by (20). The obstacle is active if

$$|f| \geq 4|\phi|$$

and, with respect of (24), the solution of Problem 1 reads

$$u(x, y) = \begin{cases} \frac{f}{4}\left(1 - x^2 - y^2\right) + A_c \ln \sqrt{x^2 + y^2} & \text{if} \quad \sqrt{x^2 + y^2} > R \\ \phi & \text{if} \quad \sqrt{x^2 + y^2} \leq R, \end{cases}$$

where

$$A_c = \frac{4\phi + fR^2 - f}{4 \ln R}.$$

An unknown contact radius $R \in (0,1)$ follows from the continuity of the first derivative

$$\frac{\partial u(r)}{\partial r}\Big|_{r=R} = 0,$$

i.e., from the nonlinear equation

$$R^2(1 - 2\ln R) = 1 - \frac{4\phi}{f}. \tag{25}$$

The corresponding energy can be expressed as

$$J(u) = \frac{\pi f^2 R^4}{16} - \frac{\pi(\phi - \frac{f}{4})^2}{16\ln R} - \frac{\pi f R^2(\phi - \frac{f}{4})}{2\ln R} - \frac{\pi f^2 R^4}{16\ln R} - \frac{\pi f^2}{16}.$$

It is not difficult to show that

$$\nabla u(x,y) = \begin{cases} \left(\frac{A_c x}{x^2 + y^2} - \frac{fx}{2}, \frac{A_c y}{x^2 + y^2} - \frac{fy}{2}\right) & \text{if} \quad \sqrt{x^2 + y^2} > R \\ (0,0) & \text{if} \quad \sqrt{x^2 + y^2} \leq R. \end{cases}$$

With respect to (8), the optimal multiplier reads

$$\lambda(x,y) = \begin{cases} 0 & \text{if} \quad \sqrt{x^2 + y^2} > R \\ -f & \text{if} \quad \sqrt{x^2 + y^2} \leq R, \end{cases}$$

so that it is a piecewise constant function.

3.2.2. Benchmark III: ring domain, spherical obstacle and zero Dirichlet BC

We replace the constant obstacle ϕ of Benchmark II by a sphere of the radius $\rho \geq 1$. An obstacle function is defined as

$$\phi(x,y) = \phi_{\max} - \rho + \sqrt{\rho^2 - x^2 - y^2},$$

where $\phi_{\max}$ is a prescribed negative constant meaning the maximal value of the obstacle function. Analogically to Benchmark II, for smaller loadings satisfying

$$|f| < 4|\phi_{\max}|$$

we have a linear problem with inactive obstacle, the solution of Problem 1 is given by (19) and corresponding energy by (20). The obstacle is active if
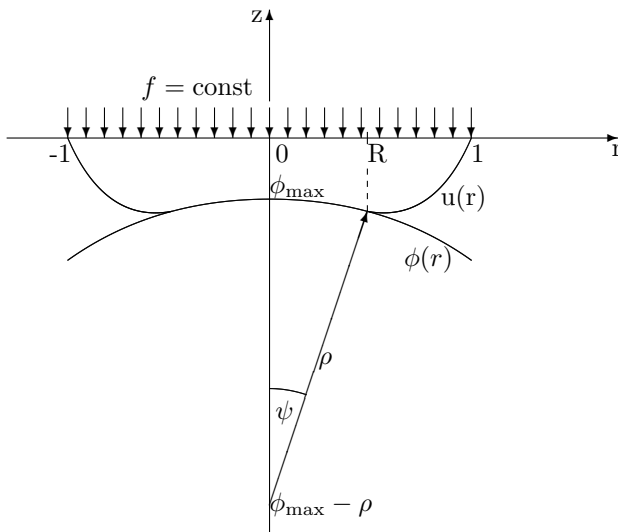
$$|f| \geq 4|\phi_{\max}|$$

holds. Then, the solution of Problem 1 reads

$$u(x,y) = \begin{cases} \frac{f}{4}\left(1 - x^2 - y^2\right) + A_s \ln\sqrt{x^2 + y^2} & \text{if} \quad \sqrt{x^2 + y^2} > R \\ \phi_{\max} - \rho + \sqrt{\rho^2 - x^2 - y^2} & \text{if} \quad \sqrt{x^2 + y^2} \leq R, \end{cases}$$

where

$$A_s = \frac{4(\phi_{\max} - \rho + \rho\cos\psi) + fR^2 - f}{4\ln R}.$$

Fig. 1. Benchmark setup: Forces f pressing an elastic membrane
against a lower spherical obstacle ϕ. The membrane displacement
$u(r)$ is displayed together with the contact radius $R = \rho \sin \psi$, where ρ
is a sphere radius and ψ an angular parameter.

An unknown contact radius $R = \rho \sin \psi$ for some angular parameter $\psi \in (0, \arcsin \frac{1}{\rho})$
(see Figure 1 for details) follows from the condition of continuity of the first derivative

$$\frac{\partial u(r)}{\partial r}\Big|_{r=R} = -\tan \psi,$$

i.e., from the solution of the nonlinear equation

$$\frac{4(\phi_{\max} - \rho + \rho \cos \psi) + f\rho^2 \sin^2 \psi - f}{4\rho \sin \psi \ln(\rho \sin \psi)} - \frac{f\rho \sin \psi}{2} = -\tan \psi. \tag{26}$$

The corresponding energy (2) can be decomposed as

$$J(u) = J_1(u) + J_2(u),$$

where the first term related to the contact domain $\Omega_\ominus^u = \{(x,y) \in \mathbb{R}^2 : x^2 + y^2 \leq R\}$
reads

$$J_1(u) = \frac{1}{2} \int_{\Omega_\ominus^u} \frac{x^2 + y^2}{\rho^2 - x^2 - y^2} \, \mathrm{d}x - \int_{\Omega_\ominus^u} f\left(\phi - \rho + \sqrt{\rho^2 - x^2 - y^2}\right) \mathrm{d}x$$

and the second term related to the remaining part $\Omega_0^u := \Omega \setminus \Omega_\ominus^u$ reads

$$J_2(u) = \frac{1}{2} \int_{\Omega_0^u} \left[\frac{A_s^2}{x^2 + y^2} - A_s f + \frac{f^2}{4} \left(x^2 + y^2 \right) \right] \, \mathrm{d}x$$

$$- \int_{\Omega_0^u} \left[\frac{f^2}{4} \left(1 - x^2 - y^2 \right) + A_s f \ln \sqrt{x^2 + y^2} \right] \, \mathrm{d}x.$$

Both terms can be further expressed as

$$J_1(u) = -\frac{\pi \rho^2}{2} [\sin^2 \psi + \ln(\cos^2 \psi)] - \pi f \rho^2 (\phi - \rho) \sin^2 \psi - \frac{2\pi f \rho^3}{3} \left(1 - \sqrt{(1 - \sin^2 \psi)^3} \right),$$

$$J_2(u) = -\pi A_s^2 \ln R - \frac{\pi f (2A_s - 1)(1 - R^2)}{4} - \frac{A_s \pi f R^2 (1 - 2 \ln R)}{2} + \frac{3\pi f^2 (1 - R^4)}{16}.$$

It is not difficult to show that

$$\nabla u(x, y) = \begin{cases} \left(\frac{A_s x}{x^2 + y^2} - \frac{fx}{2}, \frac{A_s y}{x^2 + y^2} - \frac{fy}{2} \right) & \text{if} \quad \sqrt{x^2 + y^2} > R \\ \left(-\frac{x}{\sqrt{\rho^2 - x^2 - y^2}}, -\frac{y}{\sqrt{\rho^2 - x^2 - y^2}} \right) & \text{if} \quad \sqrt{x^2 + y^2} \le R. \end{cases}$$

With respect to (8), the optimal multiplier reads

$$\lambda(x, y) = \begin{cases} 0 & \text{if} \quad \sqrt{x^2 + y^2} > R \\ \frac{2\rho^2 - x^2 - y^2}{(\rho^2 - x^2 - y^2)^{\frac{3}{2}}} - f & \text{if} \quad \sqrt{x^2 + y^2} \le R. \end{cases}$$

Remark 3.1. Existence of the first continuous derivatives $\frac{\partial u(r)}{\partial r}\big|_{r=R}$ resulting in conditions (25) and (26) to determine the contact radius R can be justified by Remark 2.2.

4. DISCRETIZATION AND NUMERICAL RESULTS

We verify the energy estimate (10) and the majorant estimate (12) on three above introduced benchmarks. Numerical experiments are based on an own implementation of the finite element method in two dimensions. A MATLAB code is available for download as a package *Obstacle problem in 2D and its a posteriori error estimate* at Matlab Central under `http://www.mathworks.com/matlabcentral/fileexchange/authors/37756`. The implementation is based on vectorization techniques of [19] and works fast even for finer rectangular meshes.

4.1. Discretization by the finite element method

The following discretizations are considered:

- the solution $v \in V_0$ of the obstacle problem is discretized in the finite dimensional subspace of bilinear nodal basis functions $V_{0,h}$ satisfying homogeneous Dirichlet boundary conditions,

- the flux $\tau^* \in H(\Omega, \text{div})$ of the majorant minimization problem is discretized in the finite dimensional subspace Q_h of the lowest order edge Raviart–Thomas functions,

- the Lagrange multiplier $\mu \in \Lambda$ of the majorant minimization problem is discretized in the finite dimensional subspace Λ_h of the elementwise constant functions.

Let us provide more implementation details. The discrete approximation $v \in V_{0,h}$ of the solution u of Problem 1 is expressed by a linear combination

$$v = \sum_{j=1}^{N} v_j \psi_j$$

of nodal bilinear functions ψ_j, where N denotes a number of nodes of a considered rectangulation $\mathcal{T}$. Nodal components are assembled in a nodal (column) vector

$$\mathbf{v} = (v_1, \dots, v_N)^T.$$

Let us assume that $N - N_D$ internal nodes are ordered first and N_D boundary Dirichlet nodes last. Then, $\mathbf{v}$ solves a quadratic minimization problem

$$\mathbf{v} = \operatorname*{argmin}_{w_i \geq \phi_i, w_j = u_j} \left\{ \frac{1}{2} \mathbf{w}^T \mathbf{K}^{BIL} \mathbf{w} - \mathbf{b}^T \mathbf{w} \right\}, \tag{27}$$

for $i \in \{1, \dots, N - N_D\}$ and $j \in \{N - N_D + 1, \dots, N\}$. Here ϕ_i and u_j denote nodal obstacle values and nodal Dirichlet boundary values. A stiffness matrix $\mathbf{K}^{BIL} \in \mathbb{R}^{N \times N}$ and a discretized loading (column) vector $\mathbf{b} = (b_1, \dots, b_N)^T \in \mathbb{R}^N$ are constructed elementwise as

$$(\mathbf{K}^{BIL})_{ij} = \int_\Omega \nabla \psi_i \cdot \nabla \psi_j \, \mathrm{d}x, \qquad b_i = \int_\Omega f \psi_i \, \mathrm{d}x \tag{28}$$

for $i, j \in \{1, \dots, N\}$. In all quadratures related to f function, f is replaced by a piecewise constant function $\bar{f}$ computed as the average of four nodal values on a rectangle. We apply the built-in Matlab function *quadprog* to solve (27).

A discretized version of Algorithm 1 is applied for the minimization of the functional majorant. The minimal flux argument $\tau_{k+1}^* \in Q_h$ in step (i) of Algorithm 1 is expressed by a linear combination

$$\tau_{k+1}^* = \sum_{j=1}^{M} y_j \eta_j,$$

of edge Raviart–Thomas vector functions η_j, where M denotes a number of rectangulation edges. The coefficient (column) vector

$$\mathbf{y} = (y_1, \dots, y_M)^T$$

solves (see (14)) a linear system of equations

$$\left[(1 + \beta_k) \mathbf{M}^{RT0} + \left(1 + \frac{1}{\beta_k} \right) \mathbf{K}^{RT0} \right] \mathbf{y} = (1 + \beta_k) \mathbf{c} - \left(1 + \frac{1}{\beta_k} \right) \mathbf{d}. \tag{29}$$

Here, a stiffness matrix $\mathbf{K}^{RT0} \in \mathbb{R}^{M \times M}$ and a mass matrix $\mathbf{M}^{RT0} \in \mathbb{R}^{M \times M}$ are constructed as

$$(\mathbf{K}^{RT0})_{ij} = \int_\Omega \mathrm{div}\eta_i \; \mathrm{div}\eta_j \, \mathrm{d}x, \qquad (\mathbf{M}^{RT0})_{ij} = \int_\Omega \eta_i \cdot \eta_j \, \mathrm{d}x$$

for $i, j \in \{1, \ldots, M\}$ and $\mathbf{c} = (c_1, \ldots, c_M)^T \in \mathbb{R}^M$ and $\mathbf{d} = (d_1, \ldots, d_M)^T \in \mathbb{R}^M$ are (column) vectors constructed as

$$c_i = \int_\Omega \nabla v \cdot \eta_i \mathrm{d}x, \quad d_i = \int_\Omega (f + \mu_k)\mathrm{div}\eta_i \, \mathrm{d}x$$

for $i \in \{1, \ldots, M\}$. No boundary conditions are imposed on $\mathbf{y}$ in (29) since the discrete solution v satisfies Dirichlet boundary conditions only. The minimal argument $\mu_{k+1} \in \Lambda_h$ in step (ii) of Algorithm 1 is computed locally on every rectangle from the formula

$$\mu_{k+1} = \left[-\mathrm{div}\,\tau_{k+1}^* - \overline{f} - \frac{\overline{v} - \overline{\phi}}{C_\Omega^2 \left(1 + \frac{1}{\beta_k}\right)} \right]^+, \tag{30}$$

where $\overline{v}, \overline{\phi}$ represent averaged rectangular values computed as the average of four nodal values on a rectangle and $[\cdot]^+ = \max\{0, \cdot\}$ denotes the maximum operator.

Remark 4.1. Exact forms of local finite element matrices are reported in Appendix.

Lemma 4.2. (Discrete convergence of the majorant minimization algorithm) Let $v \in V_{0,h}$ such that $v \neq 0$. Then, the Algorithm 1 generates a converging sequence of majorant values

$$\{\mathcal{M}(v, f, \phi; \beta_k, \mu_k, \tau_k^*)\}_{k=0}^\infty$$

and there exists majorant parameters $\tau_{\lim}^* \in Q_h$, $\mu_{\lim} \in \Lambda_h$ and $\beta_{\lim} \geq 0$ such that

$$\mathcal{M}(v, f, \phi; \beta_k, \mu_k, \tau_k^*) \to \mathcal{M}(v, f, \phi; \beta_{\lim}, \mu_{\lim}, \tau_{\lim}^*) \qquad \text{as } k \to \infty.$$

P r o o f. For any nonzero function $v \in V_{0,h}$, there is always a strictly positive distance of ∇v to the space Q_h in Ω-norm. In particular, it holds

$$\|\nabla v - \tau_k^*\|_\Omega > 0 \tag{31}$$

and all iterations β_k given by (16) are correctly defined.

Algorithm 1 generates a nonincreasing sequence of nonnegative majorant values and therefore

$$\mathcal{M}(v, f, \phi; \beta_k, \mu_k, \tau_k^*) \to \mathcal{M}_{\lim} \qquad \text{as } k \to \infty. \tag{32}$$

Consequently, the nonnegative majorant terms

$$\mathcal{M}_1(v, f, \phi; \beta_k, \mu_k, \tau_k^*) = \frac{1 + \beta_k}{2} \|\nabla v - \tau_k^*\|_\Omega^2 \tag{33}$$

$$\mathcal{M}_2(v, f, \phi; \beta_k, \mu_k, \tau_k^*) = \frac{1}{2}\left(1 + \frac{1}{\beta_k}\right) C_\Omega^2 \|\mathrm{div}\,\tau_k^* + f + \mu_k\|_\Omega^2 \tag{34}$$

are bounded. Then, the boundedness of the sequence $\{\tau_k^*\}$ in Ω-norm follows from the boundedness of the first majorant term (33). Since Q_h is finite-dimensional, the sequence $\{\tau_k^*\}$ has a converging subsequence $\{\tau_{k_m}^*\}$ denoted as $\{\tau_m^*\}$ and

$$\tau_m^* \to \tau_{\lim}^* \qquad \text{as } m \to \infty,$$

$$\operatorname{div} \tau_m^* \to \operatorname{div} \tau_{\lim}^* \qquad \text{as } m \to \infty.$$

The boundedness of the sequence $\{\mu_m\}$ in Ω-norm follows from the boundedness of the second majorant term (34). Since Λ_h is finite-dimensional, the sequence $\{\mu_m\}$ has a converging subsequence $\{\mu_{m_l}\}$ denoted as $\{\mu_l\}$ and

$$\mu_l \to \mu_{\lim} \in \Lambda_h \qquad \text{as } l \to \infty.$$

Since $\|\nabla v - \tau_l^*\|_\Omega \to \|\nabla v - \tau_{\lim}^*\|_\Omega > 0$ and $\|\operatorname{div} \tau_l^* + f + \mu_l\|_\Omega \to \|\operatorname{div} \tau_{\lim}^* + f + \mu_{\lim}\|_\Omega \geq 0$ as $l \to \infty$, it follows from (16) that

$$\beta_l \to \beta_{\lim} = \frac{\|\operatorname{div} \tau_{\lim}^* + f + \mu_{\lim}\|_\Omega}{\|\nabla v - \tau_{\lim}^*\|_\Omega} < +\infty \qquad \text{as } l \to \infty.$$

Finally, it follows from continuity of the majorant (13) that

$$\mathcal{M}(v, f, \phi; \beta_l, \mu_l, \tau_l^*) \to \mathcal{M}(v, f, \phi; \beta_{\lim}, \mu_{\lim}, \tau_{\lim}^*) \qquad \text{as } l \to \infty \qquad (35)$$

and (32) and (35) implies

$$\mathcal{M}_{\lim} = \mathcal{M}(v, f, \phi; \beta_{\lim}, \mu_{\lim}, \tau_{\lim}^*).$$

$\square$

Remark 4.3. The formulation of Lemma 4.2 still admits that

$$(\tau_{\lim}^*, \mu_{\lim}, \beta_{\lim}) \neq \operatorname*{argmin}_{\tau^* \in Q_h, \mu \in \Lambda_h, \beta > 0} \mathcal{M}(v, f, \phi; \beta, \mu, \tau^*)$$

and therefore it only holds

$$\mathcal{M}(v, f, \phi; \beta_{\lim}, \mu_{\lim}, \tau_{\lim}^*) \geq \min_{\tau^* \in Q_h, \mu \in \Lambda_h, \beta > 0} \mathcal{M}(v, f, \phi; \beta, \mu, \tau^*).$$

Remark 4.4. In all numerical experiments, only two iterations of Algorithm 1 were applied in which we set $\beta_0 = 1$ and μ_0 is provided from the quadratic programming function *quadprog*. Without a good initial iteration μ_0, the number of iterations would be significantly higher as already demonstrated in 1D numerical experiments [13].

Remark 4.5. In the particular case $v = 0$, Lemma 4.2 does not state the convergence of Algorithm 1. If $\tau_{k+1}^* = 0$ additionally, it holds

$$\|\nabla v - \tau_k^*\|_\Omega = 0$$

and the exact analysis shows:

- μ_{k+1} is computed in step (ii) from (30) as $\mu_{k+1} = \left[-\overline{f} + \dfrac{\overline{\phi}}{C_\Omega^2 \left(1 + \frac{1}{\beta_k} \right)} \right]^+$.

- $\beta_{k+1} \to +\infty$ in step (iii).

- τ_{k+2}^* is computed in step (i) from the limiting linear system of equations (29) in the form $\mathbf{M}^{RT0} \mathbf{y} = \mathbf{0}$, where $\mathbf{M}^{RT0}$ is a regular matrix. Therefore, $\tau_{k+2}^* = 0$.

- μ_{k+2} is computed in step (ii) from (30) as $\mu_{k+2} = \left[-\overline{f} + \dfrac{\overline{\phi}}{C_\Omega^2} \right]^+$.

- $\beta_{k+2} \to +\infty$ in step (iii).

Obviously Algorithm 1 converges to the limit

$$(\tau_{\lim}^*, \mu_{\lim}, \beta_{\lim}) = (0, \mu_{k+2}, +\infty).$$

However, in practical computations, the extension of real values by the value $+\infty$ requires a special attention.

Remark 4.6. Generally, $0 \le \beta_k < \infty$ in Algorithm 1 and therefore

$$0 \le \beta_{\lim} < \infty.$$

If $\beta_k = 0$, then the second majorant term (34) is replaced by its limit

$$\mathcal{M}_2(v, f, \phi; \beta_k, \mu_k, \tau_k^*) \to 0 \qquad \text{as } \beta_k \to 0+$$

in the implementation.

4.2. Verification of error estimates

We verify the energy estimate (10) and the majorant estimate (12) for all three introduced benchmarks discretized on uniform rectangular meshes $\mathcal{T}_h$ generated by the uniform mesh parameter

$$h \in \left\{ \frac{1}{2}, \frac{1}{4}, \frac{1}{8}, \frac{1}{16}, \frac{1}{32}, \frac{1}{64} \right\}.$$

The (squared) error is approximately evaluated by a quadratic form

$$\| v_h - u \|_E^2 \approx (\mathbf{v}_h - \mathbf{u}_h)^T \mathbf{K}_h^{BIL} (\mathbf{v}_h - \mathbf{u}_h) \tag{36}$$

using a discrete solution vector $\mathbf{v}_h$, a nodal interpolation vector $\mathbf{u}_h$ of the exact solution u and a stiffness matrix matrix $\mathbf{K}_h^{BIL}$ on a considered mesh $\mathcal{T}_h$. The error value is further improved by evaluations of quadratic forms

$$\| v_h - u \|_E^2 \approx (\mathcal{P}_{h/2}(\mathbf{v}_h) - \mathbf{u}_{h/2})^T \mathbf{K}_{h/2}^{BIL} (\mathcal{P}_{h/2}(\mathbf{v}_h) - \mathbf{u}_{h/2}) \tag{37}$$

or

$$\| v_h - u \|_E^2 \approx (\mathcal{P}_{h/4}(\mathbf{v}_h) - \mathbf{u}_{h/4})^T \mathbf{K}_{h/4}^{BIL} (\mathcal{P}_{h/4}(\mathbf{v}_h) - \mathbf{u}_{h/4}) \tag{38}$$

using nodal prolongation matrices $\mathcal{P}_{h/2}$ and $\mathcal{P}_{h/4}$ from $\mathcal{T}_h$ to once and twice uniformly refined rectangular meshes $\mathcal{T}_{h/2}$ and $\mathcal{T}_{h/4}$ and nodal interpolations vectors $\mathbf{u}_{h/2}$ and $\mathbf{u}_{h/4}$ of the exact solution u on $\mathcal{T}_{h/2}$ and $\mathcal{T}_{h/4}$. Postprocessing of (37), (38) requires extra memory resources but proves important to keep a proper inequality sign in the energy estimate (10). The value of (38) is used in all convergence figures and all values (36), (37), (38) are prompted in the code run for comparison.

In Benchmark I, we consider the contact radius

$$R = 0.7$$

only. The finest meshes are $\mathcal{T}_{h=1/64}$ to provide the discrete solution v_h and $\mathcal{T}_{h=1/256}$ to evaluate its error $\|v_h - u\|_E$ according to (38) are characterized by mesh properties

$$\mathcal{T}_{h=1/64} :\ 16384 \text{ elements, } 16641 \text{ nodes and } 33024 \text{ edges}$$

$$\mathcal{T}_{h=1/256} :\ 262144 \text{ elements, } 263169 \text{ nodes and } 525312 \text{ edges.}$$

Figures 2 and 3 display the discrete solution, a discrete flux component in x-direction and a discrete multiplier computed from the majorant minimization algorithm (Algorithm 1) on the rectangular mesh $\mathcal{T}_{h=1/16}$. This mesh is not the finest mesh available but it is coarse enough to stress out the shape of applied finite elements. A discrete flux component in y-direction is not shown due to symmetry reasons. Local distributions of the exact error and of the functional majorant are compared in Figure 4. Local distributions of majorant parts are depicted in Figure 5. The amplitude of the first majorant part

$$\|\nabla v - \tau^*\|_\Omega^2 \tag{39}$$

is significantly higher than amplitudes of the equilibrium and nonlinear parts $\|\mathrm{div}\,\tau^* + f + \mu\|_\Omega^2$ and $\int_\Omega \mu(v - \phi)\mathrm{d}x$. The nonlinear part indicates a layer of elements located around a boundary of the contact domain corresponding to the discrete solution v. Converge behavior for all considered rectangulations is compared in Figure 6. We can see that the energy estimate (10) and the majorant estimate (12) are very sharp with valid inequalities signs.

Remark 4.7. A simplified least-square (LS) variant of the function majorant type estimate was tested on the same benchmark including a mesh adaptivity in [7]. The main difference is that nonlinear term $\int_\Omega \mu(v - \phi)\mathrm{d}x$ is considered here in order to guarantee the majorant upper bound in (12) and enhance an accurate error control.

In Benchmark II and Benchmark III, we consider the cases

$$f = -10, \phi = -1 \text{ (for Benchmark II)}$$

$$f = -10, \phi_{\max} = -1, \rho = 1.2 \text{ (for Benchmark III)}$$

only. Numerical solutions of (25) and (26) show that contact radius R is approximately $R \approx 0.5024744$ for Benchmark II and $R \approx 0.4389205$ for Benchmark III. Since our implementation runs on rectangular elements allowing a polygonal boundary only,
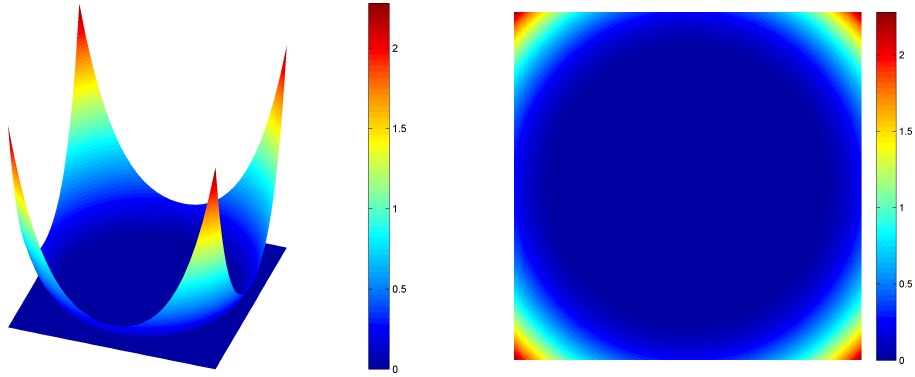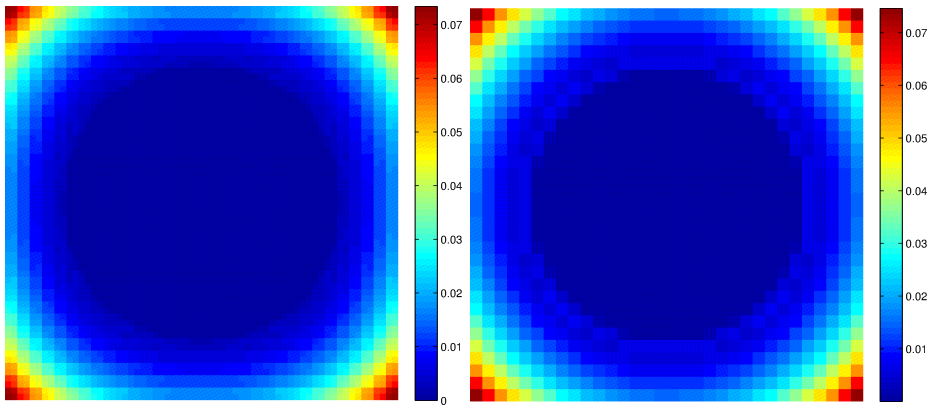
Fig. 2. Discrete solution v of the obstacle problem and the lower obstacle ϕ (left) and its rotated view (right). The dark blue color indicates the contact domain.
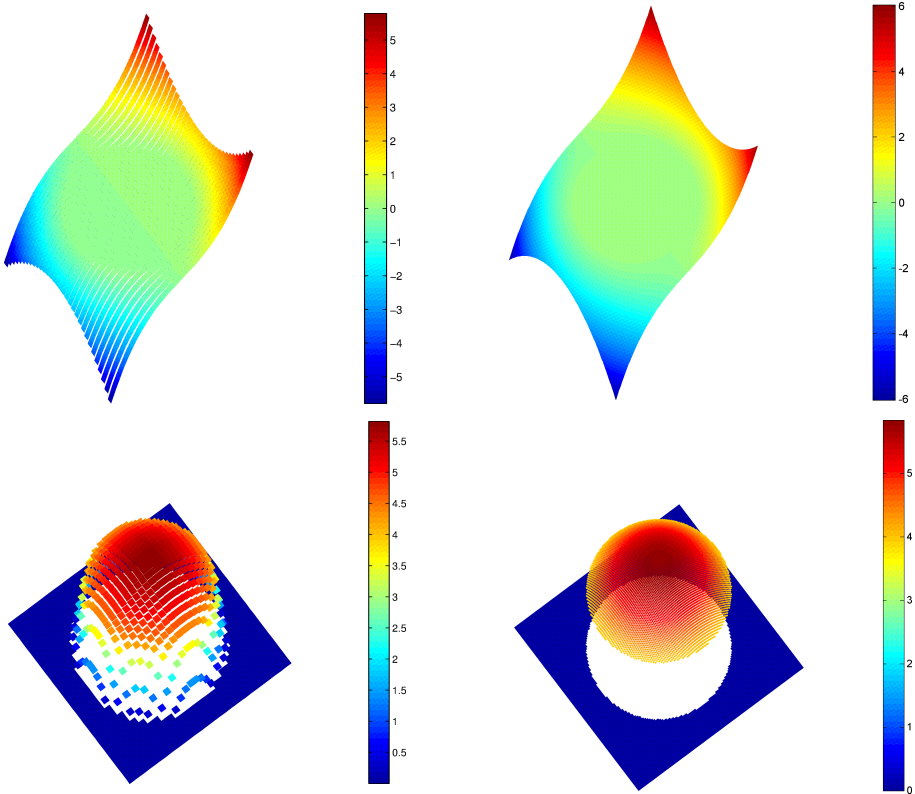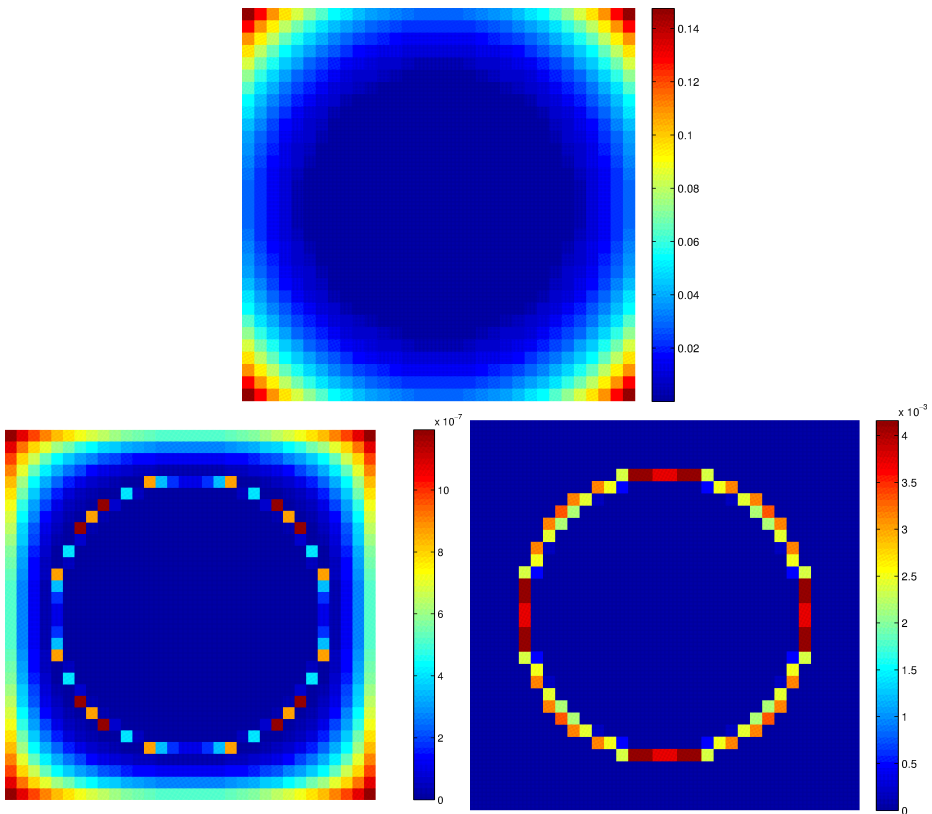

Fig. 3. Discrete flux x-component τ_x^* (top left) and discrete multiplier μ (bottom left) of the majorant minimization and exact flux x-component $\frac{\partial u}{\partial x}$ (top right) and exact multiplier λ (bottom right).
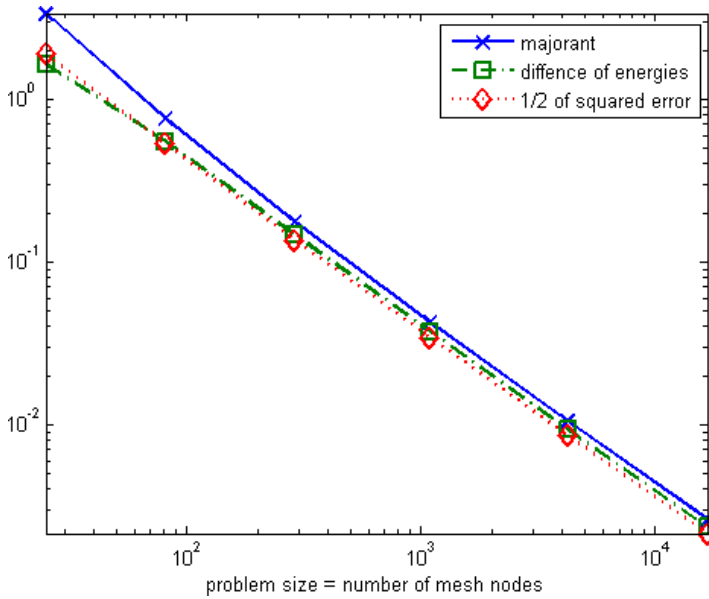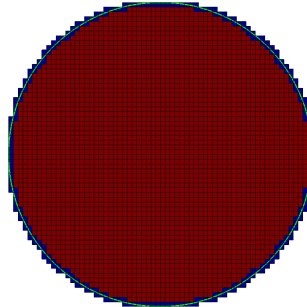
Fig. 4. Local distribution of the exact error $\frac{1}{2}\|v - u\|_E^2$ (left) and of the functional majorant $\mathcal{M}(v, \dots)$ (right).

Fig. 5. Local distributions of the functional majorant parts: $\|\nabla v - \tau^*\|_\Omega^2$ (top), $\|\operatorname{div}\tau^* + f + \mu\|_\Omega^2$ (left bottom), $\int_\Omega \mu(v - \phi)\mathrm{d}x$ (right bottom). Note that the part $\|\nabla v - \tau^*\|_\Omega^2$ contributes mostly to the functional majorant.

Fig. 6. Benchmark on a square domain with a constant obstacle: convergence.

Fig. 7. Rectangulation of the ring domain. The green line indicates the exact ring boundary, red rectangles are completely inscribed in the ring boundary and blue circumscribed rectangles contain at least one node lying outside the ring boundary. Red rectangles define an inscribed rectangulation $\mathcal{T}_\vee$ and red and blue rectangles together define a circumscribed rectangulation $\mathcal{T}^\wedge$.

we consider an inscribed rectangulation $\mathcal{T}_\vee$ and a circumscribed rectangulation $\mathcal{T}^\wedge$ as approximations of the ring boundary, see Figure 7 for details.

A discrete solution $v_\vee$ is solved on $\mathcal{T}_\vee$ satisfying zero Dirichlet boundary conditions on its boundary $\partial \mathcal{T}_\vee$. Then, $v_\vee$ is extended by zero values on $\mathcal{T}^\wedge \setminus \mathcal{T}_\vee$ (displayed by the blue color rectangles in Figure 7) to define a discrete solution $v^\wedge$ on the circumscribed rectangulations $\mathcal{T}^\wedge$. It can be easily checked that

$$J(v_\vee) := \frac{1}{2} \int_{\mathcal{T}_\vee} \nabla v_\vee \cdot \nabla v_\vee \, \mathrm{d}x - \int_{\mathcal{T}_\vee} f_\vee v_\vee \, \mathrm{d}x = \frac{1}{2} \int_{\mathcal{T}^\wedge} \nabla v^\wedge \cdot \nabla v^\wedge \, \mathrm{d}x - \int_{\mathcal{T}^\wedge} f^\wedge v^\wedge \, \mathrm{d}x := J(v^\wedge),$$

where $f_\vee$ represents a restriction of f to $\mathcal{T}_\vee$ and $f^\wedge$ represents an extension of $f_\vee$ to $\mathcal{T}^\wedge \setminus \mathcal{T}_\vee$ by any value. The extension $f^\wedge$ is defined by the same constant function f in our implementation. Finally, the majorant minimization is computed on $\mathcal{T}^\wedge$. Thus the modification of the energy estimate (10) and the majorant estimate (12) is combined in the estimate

$$\frac{1}{2} \left\| v_\vee - u|_{\mathcal{T}_\vee} \right\|_E^2 \leq J(v^\wedge) - J(u) \leq \mathcal{M}(v^\wedge, f^\wedge, \phi^\wedge; \beta, \mu^\wedge, \tau^{*\wedge}), \tag{40}$$

which is shown in convergence figures. Figures 8 and 10 display discrete solutions v of Benchmark II and Benchmark III computed on rectangulation created for $h = \frac{1}{16}$ and Figures 9 and 11 a discrete flux component in x-direction τ_x and a discrete multiplier μ computed from the majorant minimization algorithm (Algorithm 1) on the same rectangulation. Converge behaviour for all considered rectangulations is compared in Figures 12 and 13. We can see that the modified energy and majorant estimates (40) are sharp.

CONCLUSIONS

Computations for discussed benchmarks with known analytical solutions demonstrate that the functional majorant serves as a fully computable tool to estimate the upper bound of the difference of energies $J(v) - J(u)$ which serves further as an upper bound of the error in the energy norm. The majorant minimization algorithm consists of the solution of a linear system of equations for a flux variable and elementwise computation of the Lagrange multiplier. If a good a initial Lagrange multiplier field is available together with the discrete solution of the obstacle problem, the majorant minimization algorithm requires only few iterations to provide a sharp upper bound of the error.
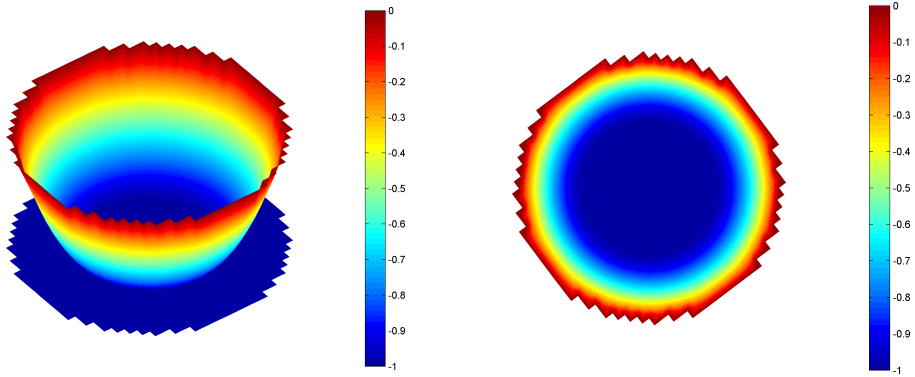
APPENDIX — LOCAL FEM MATRICES

We assume a reference rectangle T_{ref} with lengths h_x and h_y specified by vertices

$$v_1 = (0,0), \qquad v_2 = (0, h_x), \qquad v_3 = (h_x, h_y), \qquad v_4 = (0, h_y)$$

and define four local bilinear nodal basic functions

$$\hat{\psi}_1(x,y) = 1 - \frac{y}{h_y} - \frac{x}{h_x} + \frac{xy}{h_x h_y}, \qquad \hat{\psi}_2(x,y) = \frac{x}{h_x} - \frac{xy}{h_x h_y},$$

$$\hat{\psi}_3(x,y) = \frac{xy}{h_x h_y}, \qquad \hat{\psi}_4(x,y) = \frac{y}{h_y} - \frac{xy}{h_x h_y}$$

Fig. 8. Discrete solution v of the obstacle problem and the lower obstacle ϕ (left) and its rotated view (right). The dark blue color indicates the contact domain.
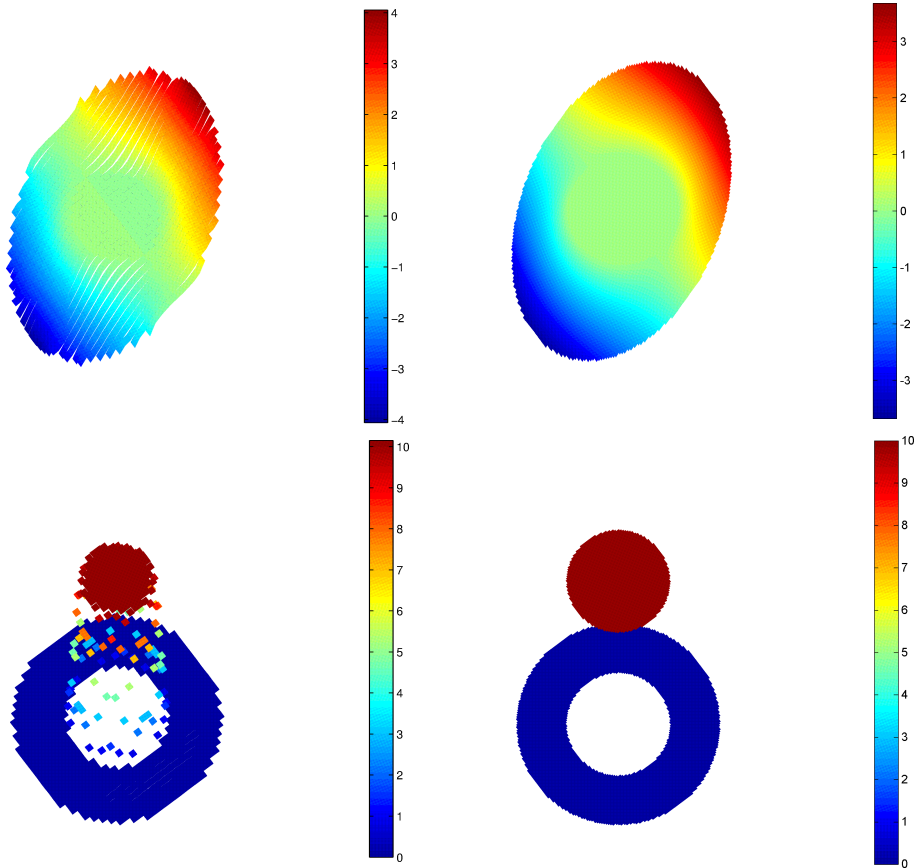
Fig. 9. Discrete flux x-component τ_x^* (top left) and discrete multiplier μ (bottom left) of the majorant minimization and exact flux x-component $\frac{\partial u}{\partial x}$ (top right) and exact multiplier λ (bottom right).
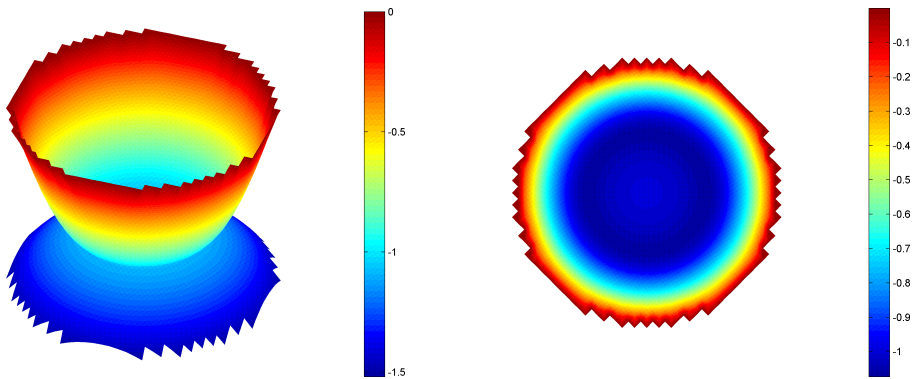
Fig. 10. Discrete solution v of the obstacle problem and the lower obstacle ϕ (left) and its rotated view (right). The dark blue color indicates the contact domain.
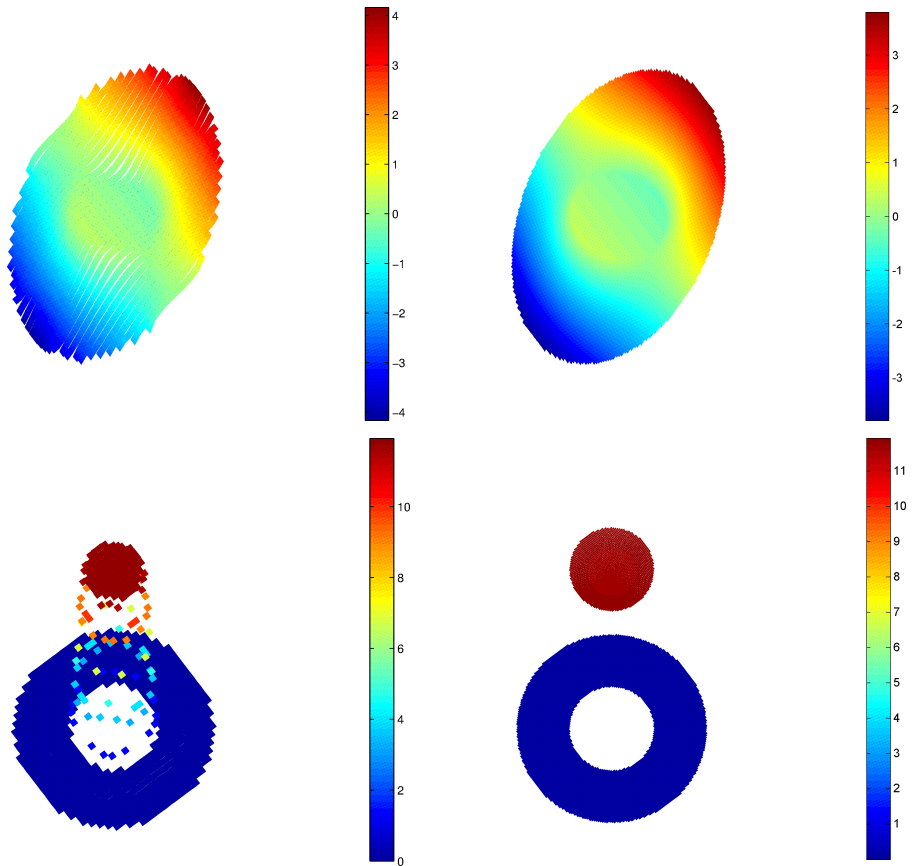
Fig. 11. Discrete flux x-component τ_x^* (top left) and discrete multiplier μ (bottom left) of the majorant minimization and exact flux x-component $\frac{\partial u}{\partial x}$ (top right) and exact multiplier λ (bottom right).
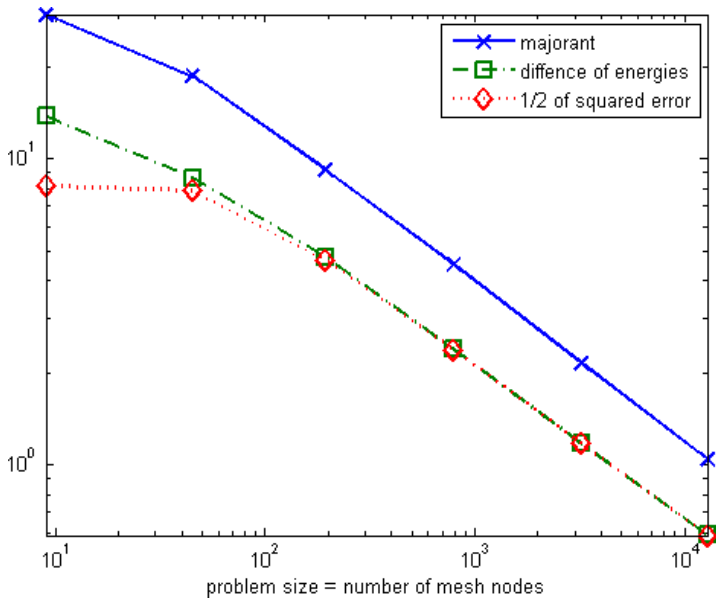
Fig. 12. Benchmark on a ring domain with a constant obstacle:
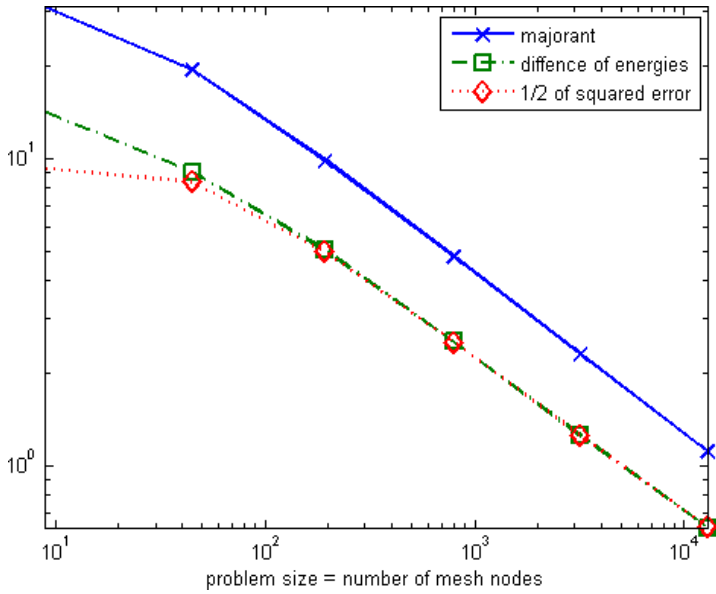convergence.

Fig. 13. Benchmark on a ring domain with a spherical obstacle:
convergence.

satisfying the relation $\hat{\psi}_i(v_j) = \delta_{ij}$ for $i, j = 1, \ldots 4$. Corresponding gradients

$$
\begin{aligned}
\nabla\hat{\psi}_1(x, y) &= \left(-\frac{1}{h_x} + \frac{y}{h_x h_y} \,,\; -\frac{1}{h_y} + \frac{x}{h_x h_y} \right), \\
\nabla\hat{\psi}_2(x, y) &= \left(\frac{1}{h_x} - \frac{y}{h_x h_y} \,,\; -\frac{x}{h_x h_y} \right), \\
\nabla\hat{\psi}_3(x, y) &= \left(\frac{y}{h_x h_y} \,,\; \frac{x}{h_x h_y} \right), \\
\nabla\hat{\psi}_4(x, y) &= \left(-\frac{y}{h_x h_y} \,,\; \frac{1}{h_y} - \frac{x}{h_x h_y} \right)
\end{aligned}
$$

are linear functions. Local stiffness matrix is defined as

$$
(\mathbf{K}_{\mathrm{ref}}^{BIL})_{ij} = \int_{T_{\mathrm{ref}}} \nabla\hat{\psi}_i \cdot \nabla\hat{\psi}_j \, \mathrm{d}x
$$

and direct computation shows

$$
\mathbf{K}_{\mathrm{ref}}^{BIL} = \frac{1}{6h_x h_y}
\begin{pmatrix}
2h_x^2 + 2h_y^2 & h_x^2 - 2h_y^2 & -h_x^2 - h_y^2 & -2h_x^2 + h_y^2 \\
h_x^2 - 2h_y^2 & 2h_x^2 + 2h_y^2 & -2h_x^2 + h_y^2 & -h_x^2 - h_y^2 \\
-h_x^2 - h_y^2 & -2h_x^2 + h_y^2 & 2h_x^2 + 2h_y^2 & h_x^2 - 2h_y^2 \\
-2h_x^2 + h_y^2 & -h_x^2 - h_y^2 & h_x^2 - 2h_y^2 & 2h_x^2 + 2h_y^2
\end{pmatrix}.
$$

Local Raviart–Thomas basis functions (of the lowest order) are vector edge based basis functions

$$
\hat{\eta}_1(x, y) := \left(0 \,,\; 1 - \frac{y}{h_y} \right), \qquad \hat{\eta}_2(x, y) := \left(\frac{x}{h_x} \,,\; 0 \right),
$$

$$
\hat{\eta}_3(x, y) := \left(0 \,,\; \frac{y}{h_y} \right), \qquad \hat{\eta}_4(x, y) := \left(1 - \frac{x}{h_x} \,,\; 0 \right)
$$

defined on reference edges

$$
e_1 = \{v_1, v_2\}, \qquad e_2 = \{v_2, v_3\}, \qquad e_3 = \{v_3, v_4\}, \qquad e_4 = \{v_4, v_1\}
$$

and they satisfy the relation $\hat{\eta}_i|_{e_j} \cdot n_j = \delta_{ij}$, where global normals n_j related to edges e_j are always oriented in directions of the coordinate system,

$$
n_1 = (0, 1), \quad n_2 = (1, 0), \quad n_3 = (0, 1), \quad n_4 = (1, 0).
$$

This choice of global normals leads to a simpler implementation with no issues related to global orientation of edges. The corresponding divergences

$$
\operatorname{div}\hat{\eta}_1 = -\frac{1}{h_y}, \quad \operatorname{div}\hat{\eta}_2 = \frac{1}{h_x}, \quad \operatorname{div}\hat{\eta}_3 = \frac{1}{h_y}, \quad \operatorname{div}\hat{\eta}_4 = -\frac{1}{h_x}
$$

are constant functions. Local stiffness and mass matrices defined by relations

$$
(\mathbf{K}_{\mathrm{ref}}^{RT0})_{ij} = \int_{T_{\mathrm{ref}}} \operatorname{div}\hat{\eta}_i \, \operatorname{div}\hat{\eta}_j \, \mathrm{d}x, \qquad (\mathbf{M}_{\mathrm{ref}}^{RT0})_{ij} = \int_{T_{\mathrm{ref}}} \hat{\eta}_i \cdot \hat{\eta}_j \, \mathrm{d}x
$$

read

$$\mathbf{K}_{\mathrm{ref}}^{RT0} = \begin{pmatrix} \frac{h_x}{h_y} & -1 & -\frac{h_x}{h_y} & 1 \\ -1 & \frac{h_y}{h_x} & 1 & -\frac{h_y}{h_x} \\ -\frac{h_x}{h_y} & 1 & \frac{h_x}{h_y} & -1 \\ 1 & -\frac{h_y}{h_x} & -1 & \frac{h_y}{h_x} \end{pmatrix}, \qquad \mathbf{M}_{\mathrm{ref}}^{RT0} = h_x h_y \begin{pmatrix} \frac{1}{3} & 0 & \frac{1}{6} & 0 \\ 0 & \frac{1}{3} & 0 & \frac{1}{6} \\ \frac{1}{6} & 0 & \frac{1}{3} & 0 \\ 0 & \frac{1}{6} & 0 & \frac{1}{3} \end{pmatrix}.$$

ACKNOWLEDGMENT

R E F E R E N C E S

[1] M. Ainsworth and J. T. Oden: A Posteriori Error Estimation in Finite Element Analysis. Wiley and Sons, New York 2000.

[2] I. Babuška and T. Strouboulis: The finite Element Method and its Reliability. Oxford University Press, New York 2001.

[3] W. Bangerth and R. Rannacher: Adaptive Finite Element Methods for Differential Equations. Birkhäuser, Berlin 2003.

[4] D. Braess, R. H. W. Hoppe, and J. Schöberl: A posteriori estimators for obstacle problems by the hypercircle method. Comput. Vis. Sci. *11* (2008), 351–362.

[5] F. Brezi, W. W. Hager, and P. A. Raviart: Error estimates for the finite element solution of variational inequalities I. Numer. Math. *28* (1977), 431–443.

[6] H. Buss and S. Repin: A posteriori error estimates for boundary value problems with obstacles. In: Proc. 3nd European Conference on Numerical Mathematics and Advanced Applications, Jÿvaskylä 1999, World Scientific 2000, pp. 162–170.

[7] C. Carstensen and C. Merdon: A posteriori error estimator competition for conforming obstacle problems. Numer. Methods Partial Differential Equations *29* (2013), 667–692.

[8] Z. Dostál: Optimal Quadratic Programming Algorithms. Springer 2009.

[9] R. S. Falk: Error estimates for the approximation of a class of variational inequalities. Math. Comput. *28* (1974), 963–971.

[10] M. Fuchs and S. Repin: A posteriori error estimates for the approximations of the stresses in the Hencky plasticity problem. Numer. Funct. Anal. Optim. *32* (2011), 610–640.

[11] R. Glowinski, J. L. Lions, and R. Trémolieres: Numerical Analysis of Variational Inequalities. North-Holland 1981.

[12] B. Gustafsson: A simple proof of the regularity theorem for the variational inequality of the obstacle problem. Nonlinear Anal. *10* (1986), 12, 1487–1490.

[13] P. Harasim AD J. Valdman: Verification of functional a posteriori error estimates for obstacle problem in 1D. Kybernetika *49* (2013), 5, 738–754.

[14] I. Hlaváček, J. Haslinger, J. Nečas, and J. Lovíšek: Solution of variational inequalities in mechanics. Applied Mathematical Sciences *66*, Springer-Verlag, New York 1988.

[15] D. Kinderlehrer and G. Stampacchia: An Introduction to Variational Inequalities and Their Applications. Academic Press, New York 1980.

[16] J. L. Lions and G. Stampacchia: Variational inequalities. Comm. Pure Appl. Math. *20* (1967), 493–519.

[17] P. Neittaanmäki and S. Repin: Reliable Methods for Computer Simulation (Error Control and A Posteriori Estimates). Elsevier, 2004.

[18] R. H. Nochetto, K. G. Seibert, and A. Veeser: Pointwise a posteriori error control for elliptic obstacle problems. Numer. Math. *95* (2003), 631–658.

[19] T. Rahman and J. Valdman: Fast MATLAB assembly of FEM matrices in 2D and 3D: nodal elements. Appl. Math. Comput. *219* (2013), 7151–7158.

[20] S. Repin: A posteriori error estimation for variational problems with uniformly convex functionals. Math. Comput. *69* (230) (2000), 481–500.

[21] S. Repin: A posteriori error estimation for nonlinear variational problems by duality theory. Zapiski Nauchn. Semin. POMI *243* (1997), 201–214.

[22] S. Repin: Estimates of deviations from exact solutions of elliptic variational inequalities. Zapiski Nauchn. Semin, POMI *271* (2000), 188–203.

[23] S. Repin: A Posteriori Estimates for Partial Differential Equations. Walter de Gruyter, Berlin 2008.

[24] S. Repin and J. Valdman: Functional a posteriori error estimates for problems with nonlinear boundary conditions. J. Numer. Math. *16* (2008), 1, 51–81.

[25] S. Repin and J. Valdman: Functional a posteriori error estimates for incremental models in elasto-plasticity. Centr. Eur. J. Math. *7* (2009), 3, 506–519.

[26] M. Ulbrich: Semismooth Newton Methods for Variational Inequalities and Constrained Optimization Problems in Function Spaces. SIAM, 2011.

[27] J. Valdman: Minimization of functional majorant in a posteriori error analysis based on $H(div)$ multigrid-preconditioned CG method. Adv. Numer. Anal. (2009).

[28] Q. Zou, A. Veeser, R. Kornhuber, and C. Gräser: Hierarchical error estimates for the energy functional in obstacle problems. Numer. Math. *117* (2012), 4, 653–677.

Petr Harasim, Brno University of Technology, Faculty of Civil Engineering, Veveří 95, 602 00 Brno. Czech Republic.
  e-mail: harasim.p@fce.vutbr.cz

Jan Valdman, Institute of Mathematics and Biomathematics, Faculty of Science, University of South Bohemia, Branišovská 31, 370 05 České Budějovice and Institute of Information Theory and Automation — Academy of Sciences of the Czech Republic, Pod Vodárenskou věží 4, 182 08 Praha 8. Czech Republic.
  e-mail: jvaldman@prf.jcu.cz